IN2P3 LPSC 06-38
CEA DAPNIA-06-04

NuFact muon storage ring : study of a triangle design based on solenoid focusing decay straights

F. Méot* and G. Rees†

June 20, 2006

Abstract

Properties of acceptance and beam transmission in a triangle design of the neutrino factory muon decay ring, with decay straights based on solenoidal focusing, are reported.

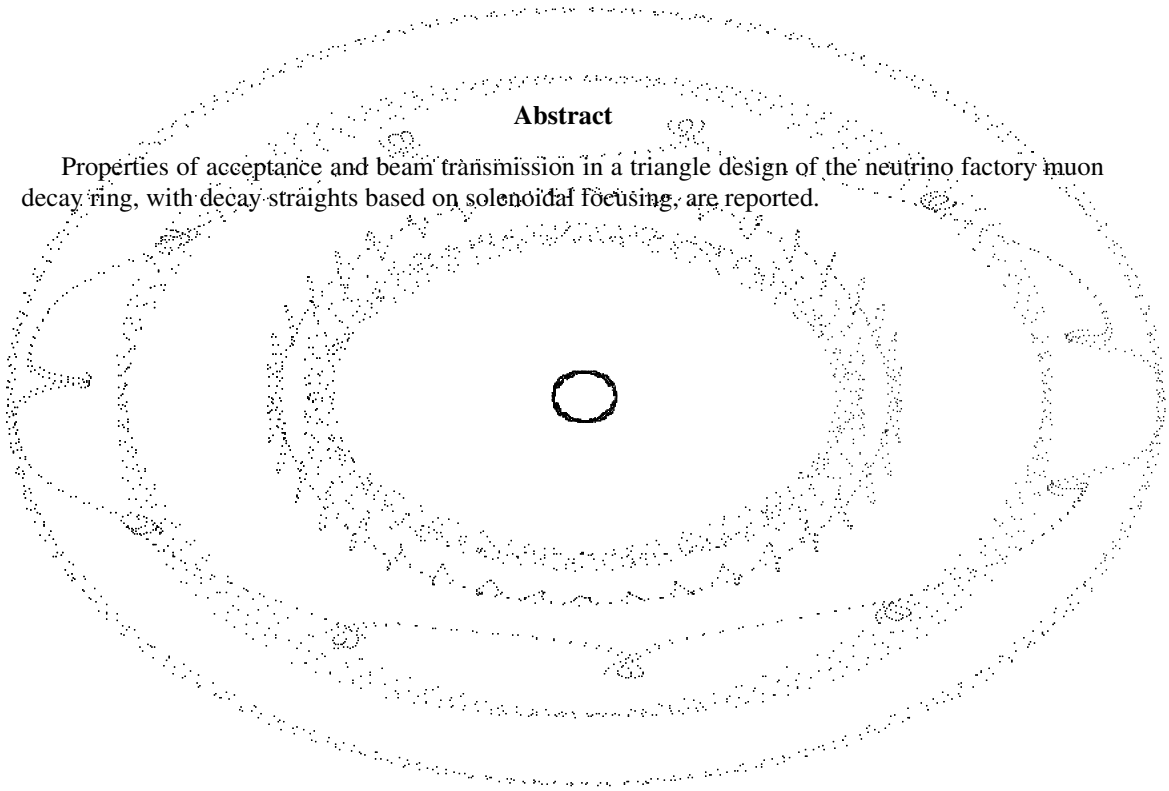

*DAPNIA&IN2P3, LPSC
†Rutherford Appleton Laboratory

Contents

1 Introduction **3**

2 Working hypothesis **3**

3 Building-up ray-tracing data **3**
3.1 Arcs . . . 5
3.2 Solenoid straight . . . 7
3.3 Tuning/Collimation/RF straight . . . 8
3.4 Full ring . . . 8
3.4.1 Beam envelopes . . . 8
3.4.2 Closed orbits . . . 9
3.4.3 Momentum dispersion (to be revisited) . . . 9
3.5 Large amplitude tracking, preliminary tests . . . 10

4 Tracking, linear machine **11**
4.1 Large amplitude tracking . . . 11
4.1.1 2-D horizontal initial conditions . . . 12
4.1.2 2-D vertical initial conditions . . . 13
4.1.3 4-D + $\delta p/p$ initial conditions . . . 14
4.2 Transmission, 4-D + $\delta p/p$, no sextupoles . . . 15
4.2.1 $\epsilon_x = \epsilon_z = 3\,\pi$ cm (norm.), $\delta p/p = \pm 1\%$. . . . 15
4.2.2 $\epsilon_x = \epsilon_z = 6\,\pi$ cm (norm.), $\delta p/p = \pm 4\%$. . . . 16

5 Transmission, 4-D + $\delta p/p$, chromaticity corrected **17**
5.1 Chromaticity correction . . . 17
5.2 Transmission . . . 17

6 Conclusion **18**

Appendix **18**

Closed orbit induced by chromaticity sextupoles **18**

References **18**

1 Introduction

The muon storage ring in the neutrino factory (NuFact in the following) is located at the high energy end of the muon acceleration chain. It delivers the μ^+/μ^- decay neutrinos to physics detectors [1].

The design of concern here, is a triangle geometry 20 GeV storage ring (upgradable to 50 GeV) (Fig. 1), parameters in Tab. 1, which features two decay straight sections, each one aiming at a distant detector. The third straight section of the ring is devoted to tuning, collimation and RF.

A particularity of the proposed design, is in its being based on solenoid focusing decay straights, which has the virtue of minimizing the betatron amplitudes, compared to equivalent quadrupole focusing. The solenoidal focusing ensures the requested ratio, for the r.m.s. divergences of the 20 GeV muon and the neutrino beam, of 0.1 for an assumed muon normalized r.m.s. emittance of $4800\,\pi$ mm mr ($3\,\pi$ cm, total).

The goal of the present work is to show the viability of this design, in particular as concerns the impact of the solenoid focusing on machine behavior. It addresses the questions of residual coupling, machine acceptance, and concludes with a computation of beam transmission over 1000 turns.

2 Working hypothesis

A description of the design principles and of the lattice can be found in Ref. [2]. Unless otherwise mentioned, working conditions, design parameters, etc., refer to it. The present study is based on stepwise ray-tracing [3], for the sake of accuracy in the representation of magnetic fields (combined function dipoles, solenoids, fringe fields, etc.), given the very large beam emittances of concern, however two matrix optics codes are used in addition for building the ray-tracing data files, and for cross-checks, namely, BETA [4] and MAD [5].

The report is organized as follows :
Section 3 establishes the basic optical properties of the storage ring, on the basis of ray-tracing methods, with cross-checks using matrix codes, and establishes the accuracy of the thousand turns range multiturn stepwise ray-tracing. Section 4.1 describes the machine behavior in presence of largest amplitude motion. Transmission simulation results are given in Section 4.2.

Various Appendices give additional details concerning the optics, numerical data, methods.

3 Building-up ray-tracing data

Goals, methods

This preliminary Section 3 has various aims :

- ensure the correctness of the ray-tracing data and data files
- maximize the integration step sizes so to maximize the tracking speed while preserving sufficient symplecticity over about 10^4 turns in the ring (which is more than one order of magnitude larger than the storage duration).
- set up ray-tracing data that yield first order quantities : phase advances, betatron amplitudes, dispersions, etc., which stick as much as feasible to the matrix transport outputs.

Various hypothesis concerning the tracking data

- The arc dipoles are combined function magnets. This raises the question of the respective values of the dipole field and of the radial magnet positioning. These quantities can be arbitrarily chosen with the sole constraint of yielding zero closed orbit and the correct dispersion. Therefore our hypothesis in the present work is the following : the bending strength $B_0/B\rho = 1/\rho$ is taken equal to that of the reference ring [2], the ensuing positioning is determined so to cancel the closed orbit. We leave to further inspection the

Table 1 : Muon storage ring parameters.
The right column gives, where worth, the stepwise ray-tracing data.

		Matrix	Ray-tracing
Energy	(GeV)	20	
Circumference	(m)	1170.764	
Requested transverse acceptance	(π cm, norm.)	3	
Requested $\delta p/p$ acceptance	(%)	± 1	
Total tunes ν_x/ν_z		10.790 / 11.151	10.791 / 11.147
Total chromaticities ξ_x/ξ_z		-14.45 / -14.67	-14.35 / -14.92
Arcs			
10-cell arcs (2) :			
Length	(m)	78	
Deviation	(deg)	96.73	
Phase advance (μ_x/μ_z)	(2π)	2 / 2	
ξ_x/ξ_z		-2.01 / -2.27	-2.15 / -2.30
16-cell arc (1) :			
Length	(m)	124.8	
Deviation	(deg)	154.766	
Phase advance (μ_x/μ_z)	(2π)	3.2 / 3.2	
ξ_x/ξ_z		-3.21 / -3.60	-3.44 / -3.67
Arc cell :			
Length	(m)	7.8	
Phase advance (μ_x/μ_z)	(deg)	72	
$\beta_{x,z}$ max	m	12.6	
D_x max	m	1.08	
Arc cell combined function dipole :			
Length	(m)	1.25	
Deviation	(deg)	4.836	
Curvature	(1/m)	0.337647	
Foc. strength	(m^{-2})	± 0.16	
Production Straight			
Length	(m)	126	
Number of solenoids	(/straight)	8	
Solenoid field, length	(T, m)	4, 4	
Phase advance (μ_x/μ_z)	(2π)	0.5 / 0.5	
$\beta_{x,z}$ max	(m)	100	
Tuning/Collimation/RF straight Straight			
Length	(m)	148.364	
Quad. strengths	(m^{-2})	< 0.11	
Quad. lengths	(m)	110, 200, 300, 340	
Phase advance (μ_x/μ_z)	(2π)	1.62 / 2.05	
$\beta_{x/z}$ max	(m)	103 / 58	
D_x max	(m)	0.7	
Matching sections			
Phase advance (μ_x/μ_z)	(2π)	0.97 / 0.9	

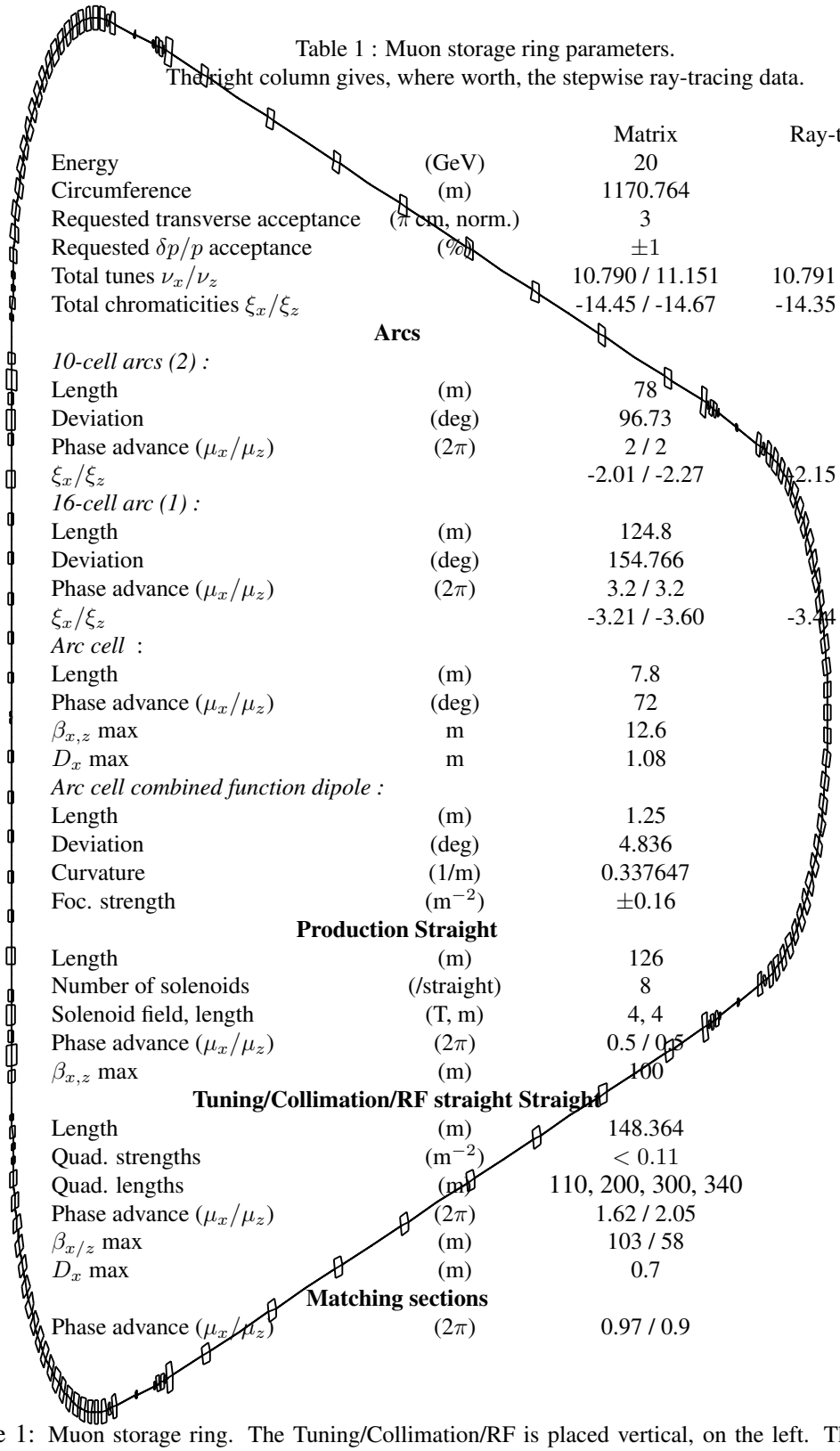

Figure 1: Muon storage ring. The Tuning/Collimation/RF is placed vertical, on the left. The 8-solenoid decay straights are the two others. The left two arcs have ten cells, the right one has 16.

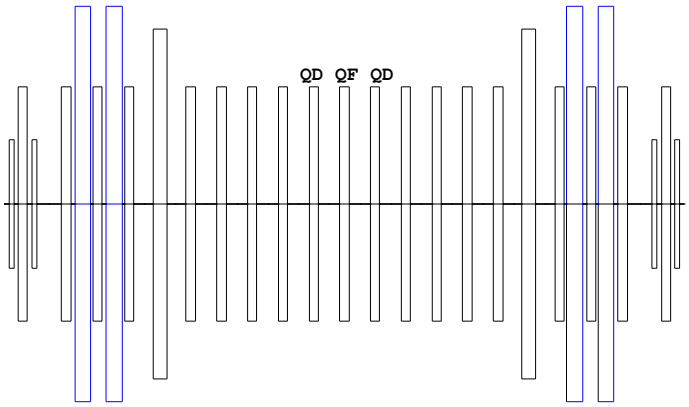

Figure 2: Tuning/Collimation/RF straight, located between the two 10-cell arcs. The section comprises 4 dipoles (blue), and quadrupoles with three different lengths. The four central cells ($\frac{1}{2}QF - QD - \frac{1}{2}QF$) are used for tune adjustment.

question of the exact reference field and positioning of these magnets.
- In this process of dipole positioning, the quadrupole components (K_1) need slight readjusting so to obtain phase advances value of Ref. [2].
- Bends are all assumed sector in Ref. [2], whereas they all are taken parallel face in the ray-tracing. However, (i) this only has very little effect on K_1, (ii) for various reasons, such as the presence of fringe fields, the phase advances of the ring pieces (arcs, decay straights, etc.) in the ray-tracing case need however be slightly readjusted so to identify with the matrix transport data ; this will take care of that sector/rectangle difference.
- Fringe fields are set in all dipoles, quadrupoles and solenoids, typical shapes are shown in Figs. 3, 5.

Choice of tunes, adjustment

They should be kept away from 3rd to 5th order resonances. Alternate values to the present ones, 10.79/11.15 (Tab. 1), can be, 10.83/11.17, 10.62/11.38, or, furthest from 5th order resonance, 10.71/11.29.

Tune adjustments are realized using the two pairs of cells ($\frac{1}{2}QF - QD - \frac{1}{2}QF$) located on both sides of the tuning straight section center, Fig. 2. Adaptation to the arc conditions is realized by buffer cells, the process requires a couple of iterations.

3.1 Arcs

The arc cell has the form

$$[D8, BFA, D8, BDA]$$

optical functions are shown in Fig. 3. The arcs have the form

$$[BDE, N * (D8, BFA, D8, BDA), D8, BFA, D8, BDE]$$

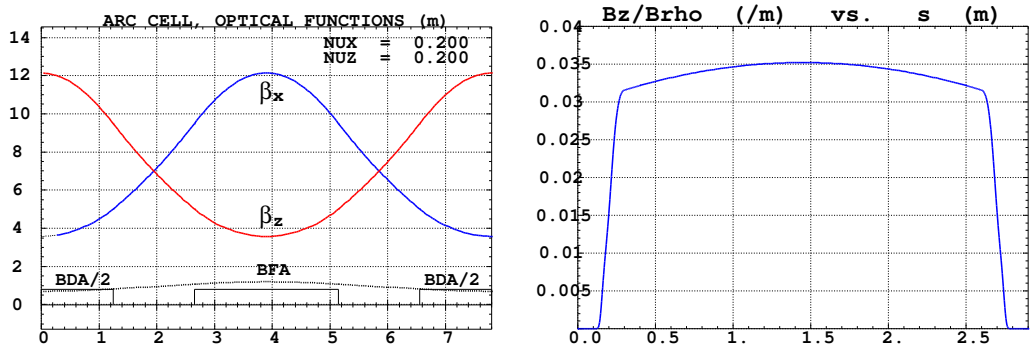

Figure 3: Left : arc cell, optical functions and periodic dispersion. Right : typical field at traversal of a combined function BFA-type dipole, including fringe fields, in the stepwise ray-tracing method.

wherein $N = 9$ or $N = 15$ for respectively the two 10-cell and the single 16-cell arcs, BDE=$\frac{1}{2}$BDA, D8 is a 1.4 m drift, and with other characteristics as described below.

Satisfactory degree of symplecticity over 10^5 passes on the maximum invariant 6 πcm in the cell is ensured using respectively 120/160/120 integration steps in the about 40 cm / 210 / 40 cm long entrance/body/exit regions of the BFA and BDA combined function dipoles. This is shown in Fig. 4. For comparison, taking 30/40/30 integration steps instead would yield horizontal phase space similar to that in Fig. 4, yet with noticeable smear in the vertical invariant.

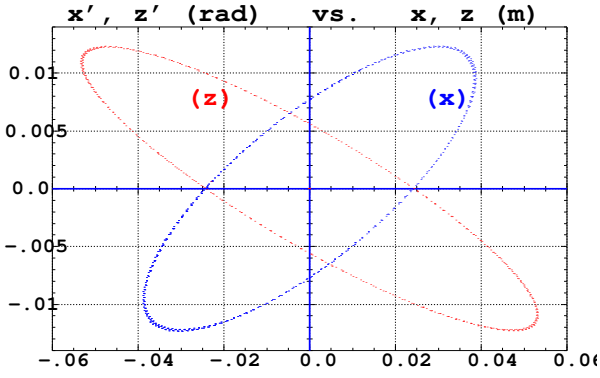

Figure 4: (x, x') and (z, z') motions, single particle, 10^5 passes in a cell, observed at ends of arc cell. Invariant values $\epsilon_x = \epsilon_z = 6$ πcm.

Table 1: Ray-tracing data concerning the arc cell, together with matrix method hypothesis for comparison.

Magnet		type	length (m)	$1/\rho$ (m^{-1})	K_1 (m^{-2})	angle (rad)	shift (10^{-2}m)
BFA	*Matrix method*	sbend	2.50	0.0337647	0.1580318	0.0844117	0
	Ray-tracing	sbend	2.50	id.	0.15917403	id.	1.78275
BDA	*Matrix method*	sbend	2.50	0.0337647	-0.1592295	0.0844117	0
	Ray-tracing	sbend	2.50	id.	-0.15817843	id.	1.72389
BDE	*Matrix method*	sbend	1.25	0.0337647	-0.1592295	0.0844117	0
	Ray-tracing	sbend	1.25	id.	-0.15817843	id.	0.4334

Chromaticity

We estimate the chromaticity using (y standing for x or z)

$$\xi_y \approx -\int \beta_y K_y ds \,/\, 4\pi \approx -N_Q(\beta_y|_{max} - \beta_y|_{min}) K_y L \,/\, 4\pi$$

From what precedes we have $K_{x,z} \approx 0.16$ m^{-2} (Tab. 1), $\beta_{x,z}|_{max} \approx 10.5$ m (Fig. 3), $\beta_{x,z}|_{min} \approx 3.5$ m, quadrupole length $L \approx 2.5$ m. This yields $\xi_x \approx \xi_z \approx -N_Q \times 2.2$, in agreement with code computations

(see parameter Table, page 4). The total chromaticities induced by the arcs are $\xi_x/\xi_z \approx -7.8/-8.3$, about half the ring values. Sextupoles located in the arc magnets will thus have to compensate twice the arc chromaticities. The correction can be estimated from $K_{\substack{x\\z}} \mp S_{\substack{x\\z}} D_x = 0$, however the decoupling between β_x and β_z in not so strong, so that the estimate is loose. A few iterations yield $S_x \approx 12$ m^{-3}, $S_z \approx 20$ m^{-3}.

3.2 Solenoid straight

The solenoidal focusing assumes that, the ratio for the r.m.s. divergences of the 20 GeV muon and the neutrino beam is set at 0.1 for an assumed muon, normalized, r.m.s. emittance of 4800 π mm mr.

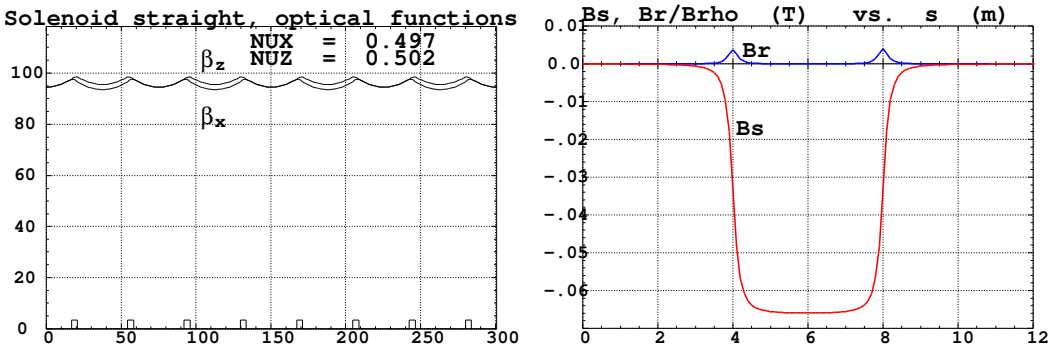

Figure 5: Left : optical functions in the solenoid straight. Right : typical field components at traversal of a solenoid, off-axis, in the stepwise ray-tracing model.

The solenoid straight ends feature series of weak bends, not shown here, the role of which is to remove the neutrinos originating from the muons which decay in the ring matching sections, of larger divergence angles.

The focal length in the solenoids satisfies

$$1/f_s == \int (B_s/2B\rho)^2 ds \approx L(B_s/2B\rho)^2$$

with L=length, B_s=longitudinal field, yielding rotation of the decoupling-free frame $\Omega = \int (B_s/2B\rho)ds \approx B_s L/2B\rho$. Again, fringe fields cause some slight difference between both with results as follows :

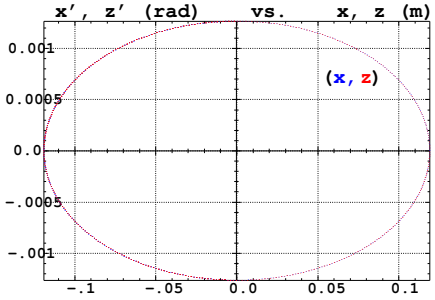

Figure 6: (x, x') and (z, z') motions, single particle, stepwise tracked over 2000 passes through the solenoid straight, observed at the straight end.

	length (m)	$B_s/2B\rho$ (m^{-1})	fall-off extent (m)
$Matrix\ method$	4	0.0318503	0
$Ray-tracing$	4	0.0331322	4

Fig. 5-left gives the beta functions along the decay straight. Fig. 5-right shows typical longitudinal (B_s) and radial (B_r) field component as experienced by a particle at traversal of a solenoid, off-axis. Fig. 6 shows the good behavior of a 2000-pass tracking through the solenoid straight. The particle has been launched on $\epsilon_x/\pi = \epsilon_z/\pi = 3\,\pi$cm invariants, the phase advance is $0.4976 \times 2\pi$ per pass. An ellipse fitting yields $\beta_x = \beta_z = 94.4$ m, $\alpha \approx 0$, as expected. The integration step size is 1 cm, the fringe field extent accounted for is 4 m at both ends of the solenoids.

3.3 Tuning/Collimation/RF straight

The optical characteristics are given in Fig. 7-left. Fig. 7-right shows the good behavior of the multiturn stepwise tracking ; matching to these ellipse yields $\beta_x = 3.65$ m, $\beta_z = 11.60$ m, $\alpha_{x,z} \approx 0$, as expected ; integration step size in quadrupole fringe field and body regions are respectively about 0.5 cm and 5 cm.

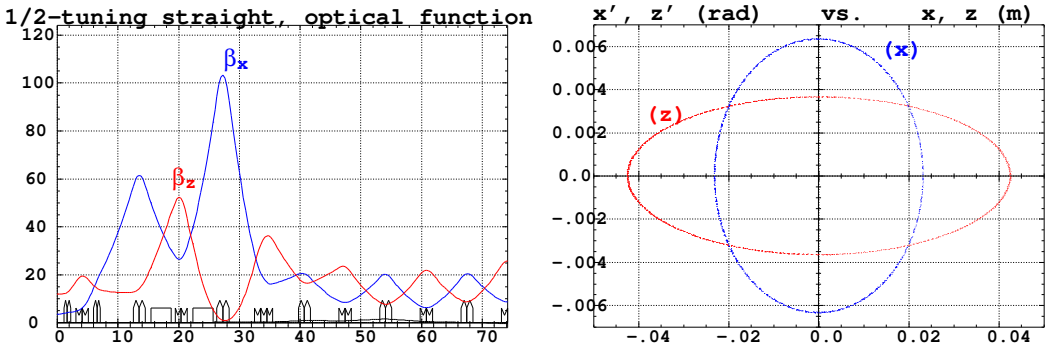

Figure 7: Left : optical functions in half the collimation/tuning/RF straight (from arc to straight center). Right : 10^4-pass tracking, single particle launched on $\epsilon_x = \epsilon_z = 3\,\pi$ cm (norm.), through the collimation straight ; x and z phase space motions are observed at straight end.

3.4 Full ring

The goal of this Section is, prior to further large amplitude and DA tracking, to show the correct behavior of the stepwise ray-tracing and multiturn tracking over the ring, in terms of first order invariants, envelopes, etc.

3.4.1 Beam envelopes

A set of 50 particles is launched, these particles are evenly spread on $\epsilon = 3\,\pi$ cm invariant, either pure (x,x') or pure (z,z') (Fig. 8), while $\delta p/p \equiv 0$. This set is tracked for a single turn. This yields the excursions along the ring, the extreme ones coinciding with the horizontal and vertical envelopes. Results are given in Fig. 8, together with envelopes obtained from matrix transport for comparison. It can be verified that the agreement is good (regardless of the slight β-beat from the matrix code in the solenoid straights).

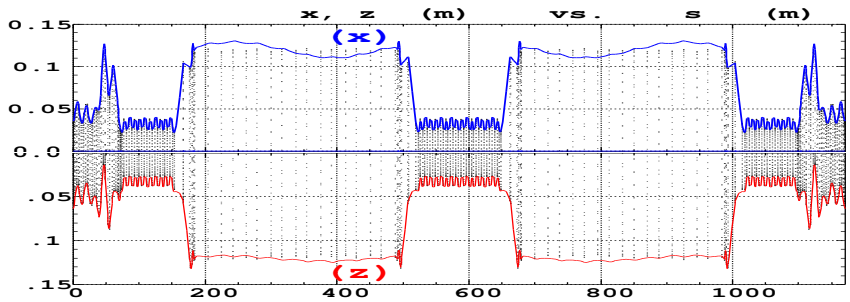

Figure 8: Beam envelopes.

3.4.2 Closed orbits

The residual geometrical closed orbits, as induced in the horizontal plane by the combined function dipoles and coupled into the vertical plane by the solenoids, are shown in Fig. 9. It can be seen that these are small, with maximum amplitude less than 0.04 mm in x and less than 0.07 mm in z.

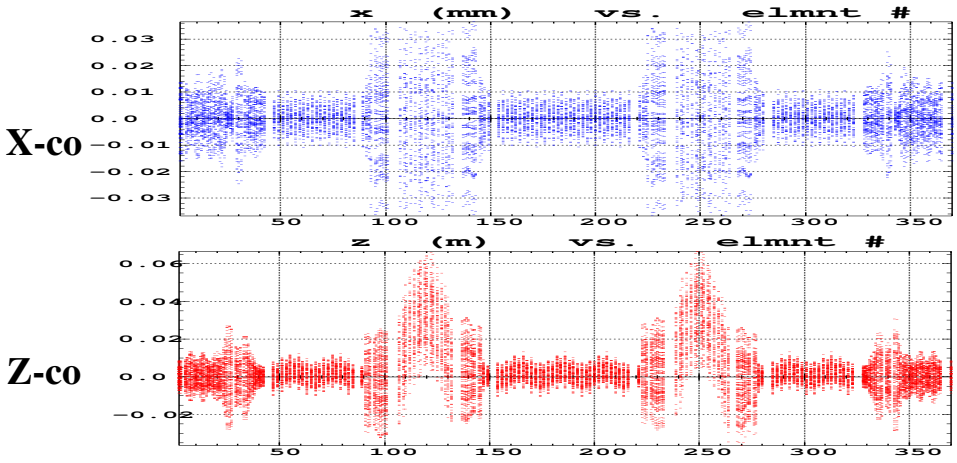

Figure 9: Residual geometrical closed orbits (horizontal axis gives optical element number).

3.4.3 Momentum dispersion (to be revisited)

Dispersion functions are obtained by tracking the closed orbit of a chromatic particle, after normalization by $\delta p/p$. They are shown in Fig. 10, they reach maximum values $D_{x,max} \approx 1.1$ m, and, due to coupling $D_{z,max} \approx 1$ mm. The agreement with matrix methods is good.

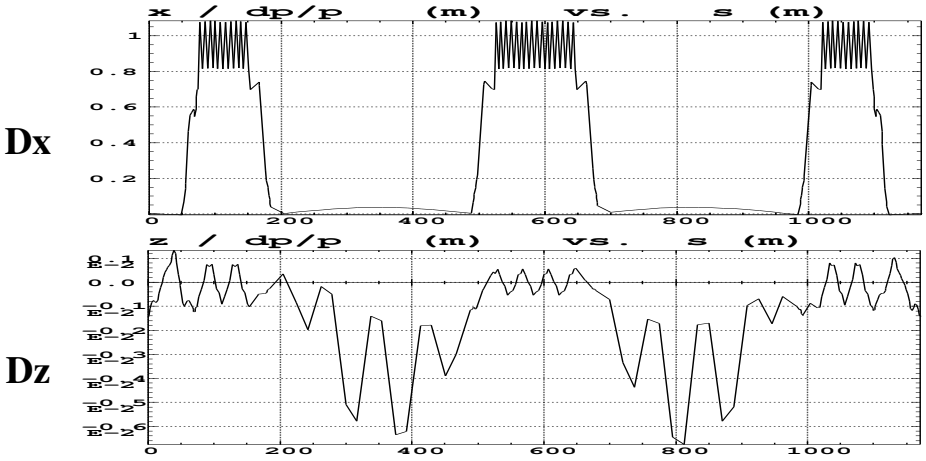

Figure 10: Chromatic closed orbits (horizontal axis gives optical element number).

3.5 Large amplitude tracking, preliminary tests

The results below have the mere goal of giving a rapid idea of expectable acceptances. They are clearly satisfactory and justify further inspection, next Sections.

In case of purely 2D initial beam coordinates, multiturn stepwise ray-tracing yields the following maximum stable amplitudes :

Maximum stable starting invariant (normalized)	induced emittance	corresponding tunes ν_x/ν_z
$\epsilon_x/\pi = 2.64 \times 3\,\pi$cm	$\epsilon_z/\pi = 0.01 \times 3\,\pi$cm	0.799 / 0.182
$\epsilon_z/\pi = 2.63 \times 3\,\pi$cm	$\epsilon_x/\pi = 0.03 \times 3\,\pi$cm	0.825 / 0.155

If now non-zero $\delta p/p$ is introduced, the maximum stable amplitudes are sensibly decrease compared to the above, due to the absence of chromaticity corrections in the present optics. This is illustrated in Fig. 11 with $\delta p/p = 0.5\%$. The corresponding tunes are shown in Fig. 12, they differ from the $\delta p/p = 0$ ones ($\nu_x = 10.79$, $\nu_z = 11.15$, Tab. 1) by the amount $\Delta\nu_{x,z} = \xi_{x,z}\delta p/p$, with $\xi_{x,z} \approx -15$.

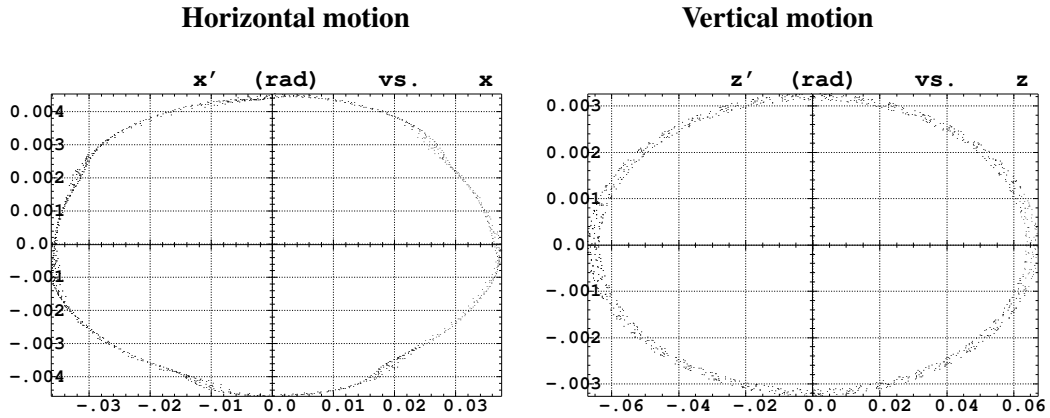

Figure 11: A particle launched on $\epsilon_x = \epsilon_z = 3.6\,\pi$ cm invariants and with $\delta p/p = 0.5\%$. 1000 turns in the ring.

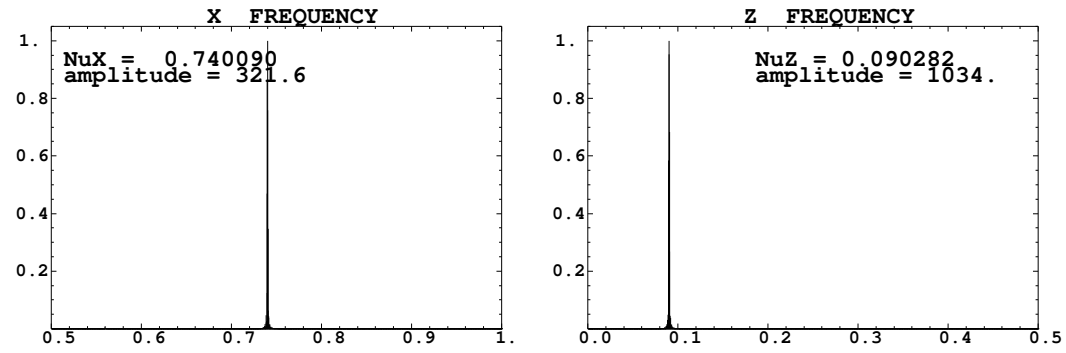

Figure 12: Corresponding spectra, victim of momentum detuning.

4 Tracking, linear machine

4.1 Large amplitude tracking

Here, we first perform a series of tests aimed at controlling the large amplitude behavior, both of the tracking method and of the ring itself. We limit the investigations to the $\epsilon_x/\pi = 3\,\pi$cm, $\epsilon_z/\pi = 3\,\pi$cm, $\delta p/p = \pm 1\%$ ranges, these will be pushed further in Section 4.2.2.

Initial conditions

Fig. 13 shows the initial distributions used in the following. They represent the beam at the middle of the tuning straight section.

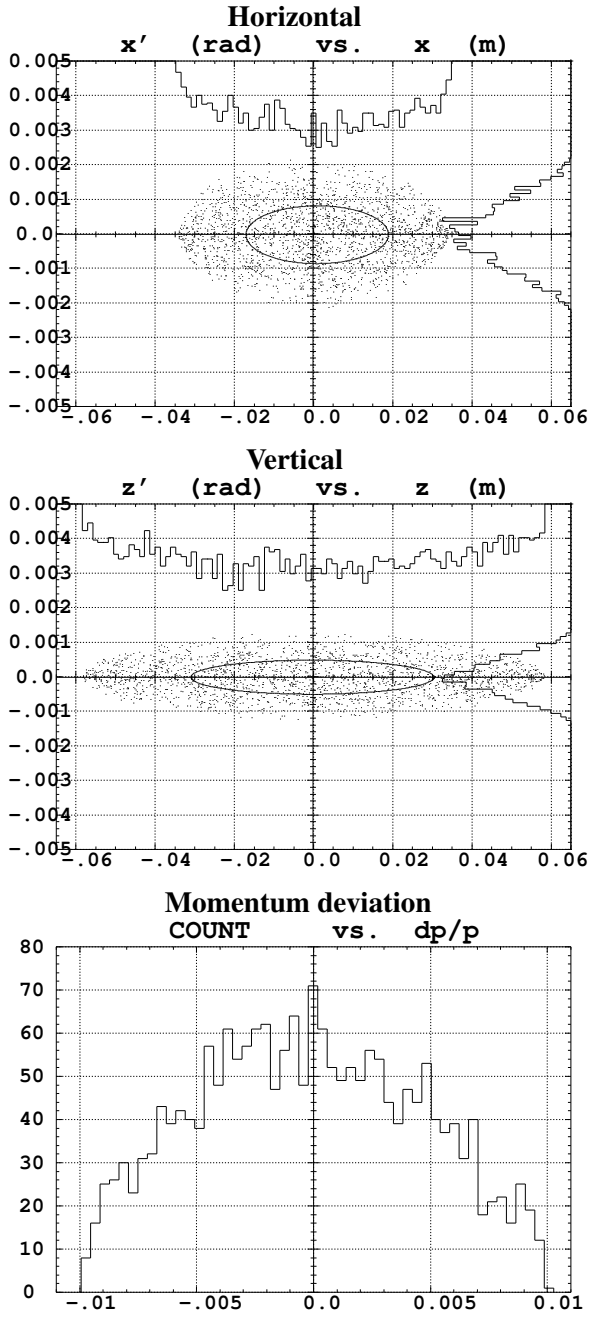

Figure 13: $\epsilon_x/\pi = 3\,\pi$cm, $\epsilon_z/\pi = 3\,\pi$cm, $\delta p/p = \pm 1\%$.

4.1.1 2-D horizontal initial conditions

An initial 200-particle beam with zero vertical initial amplitudes, initial (x, x') as shown in Fig. 13, $\delta p/p = 0$, is tracked for a few hundred turns. The transmission is 100%. Fig. 14 shows the tracking results :
- the horizontal motion (i) is highly linear, up to $\epsilon_x = 3\pi$cm here,
- the coupling is very weak given here $\nu_x/\nu_z = 10.79/11.15$ on-momentum tune values, as a consequence the vertical motion induced (ii) is very small,
- corresponding Fourier spectra are shown in Figs. 14-(iii,iv), the vertical one is very weak as expected from what precedes, and shows a side peak due to (negligible) $x - z$ coupling,
- the beam extent in the tune diagram (v) is mostly due to the chromaticities,
- in the amplitude-detuning plot, Fig. (vi), the ϵ_x/π value for each particle is drawn from *elliptical* fit of the particle motion in phase-space, which is justified, following Fig. 14-(i). The amplitude-detuning appears to be very weak, this is due to the absence of strong field non-linearities,

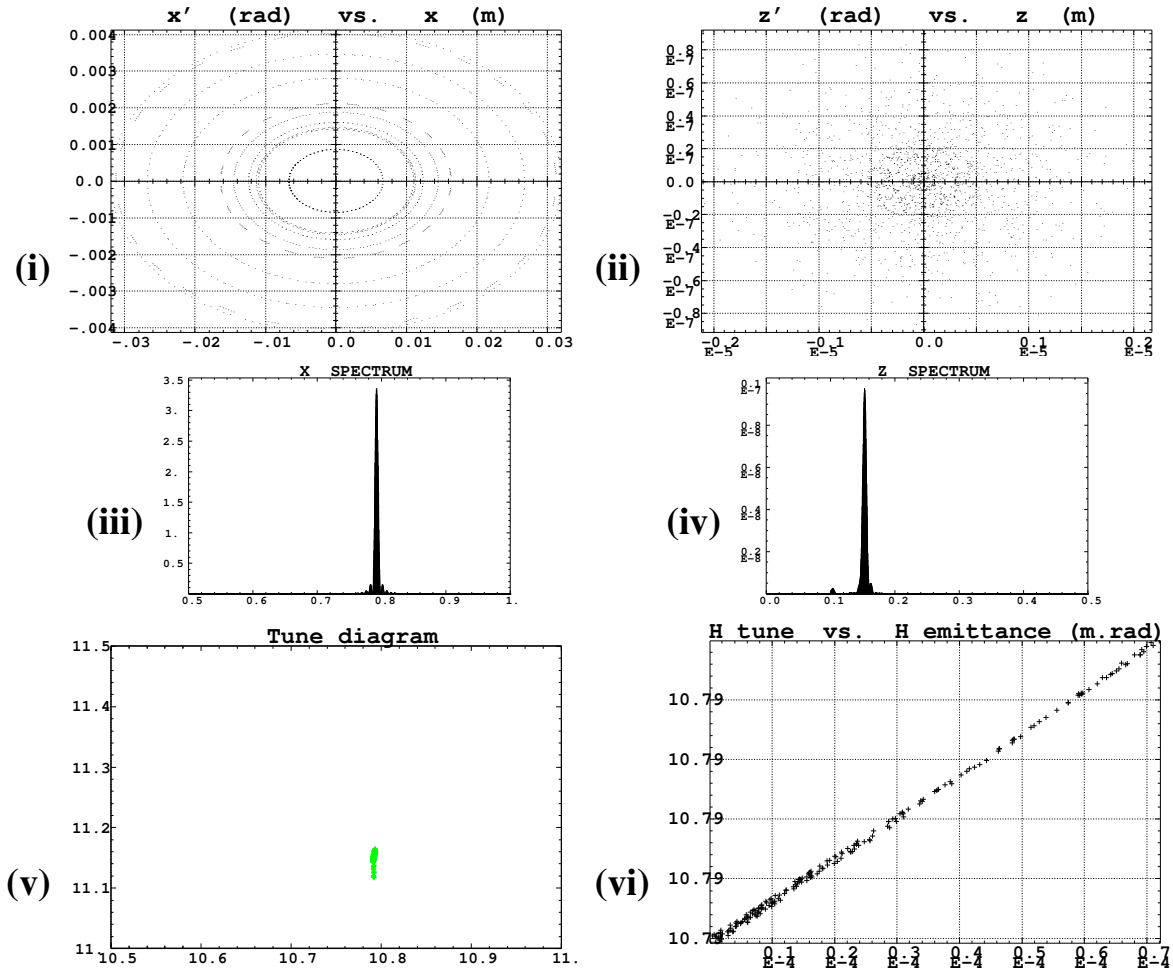

Figure 14: (i) Horizontal motion of sample particles, up to about $3\,\pi$ cm. (ii) Corresponding small vertical motion, induced by solenoidal coupling. (iii, iv) Specimen ν_x and ν_z spectra. (v) Tune diagram for the 200 particles, obtained by Fourier analysis. (vi) Amplitude detuning, ν_x as a function of ϵ_x/π.

4.1.2 2-D vertical initial conditions

An initial 200-particle mono-energetic beam, with zero horizontal initial amplitude, $\delta p/p = 0$, initial (z, z') distributed as shown in Fig. 13, $\epsilon_z = 3\pi$cm (norm.), is tracked for a few hundred turns over the ring. The transmission is 100%. Fig. 15 shows the tracking results :

- the vertical motion (ii) is highly linear, up to $\epsilon_z = 3\pi$cm here,

- the coupling is very weak given here $\nu_x/\nu_z = 10.79/11.15$ on-momentum tune values, as a consequence the horizontal motion induced (i) is very small,

- corresponding Fourier spectra (iii,iv) : the horizontal one is very weak, and shows a side peak on the left, due to the $x - z$ coupling,

- the beam extent in the tune diagram (v) is mostly due to the chromaticities,

- in the amplitude-detuning plot in Fig. 14-vi, the ϵ_z/π value for each particle is drawn from *elliptical* fit of the particle motion in phase-space, which is justified, see Fig. (ii). The amplitude-detuning appears to be very weak, this is due to the absence of strong field non-linearities,

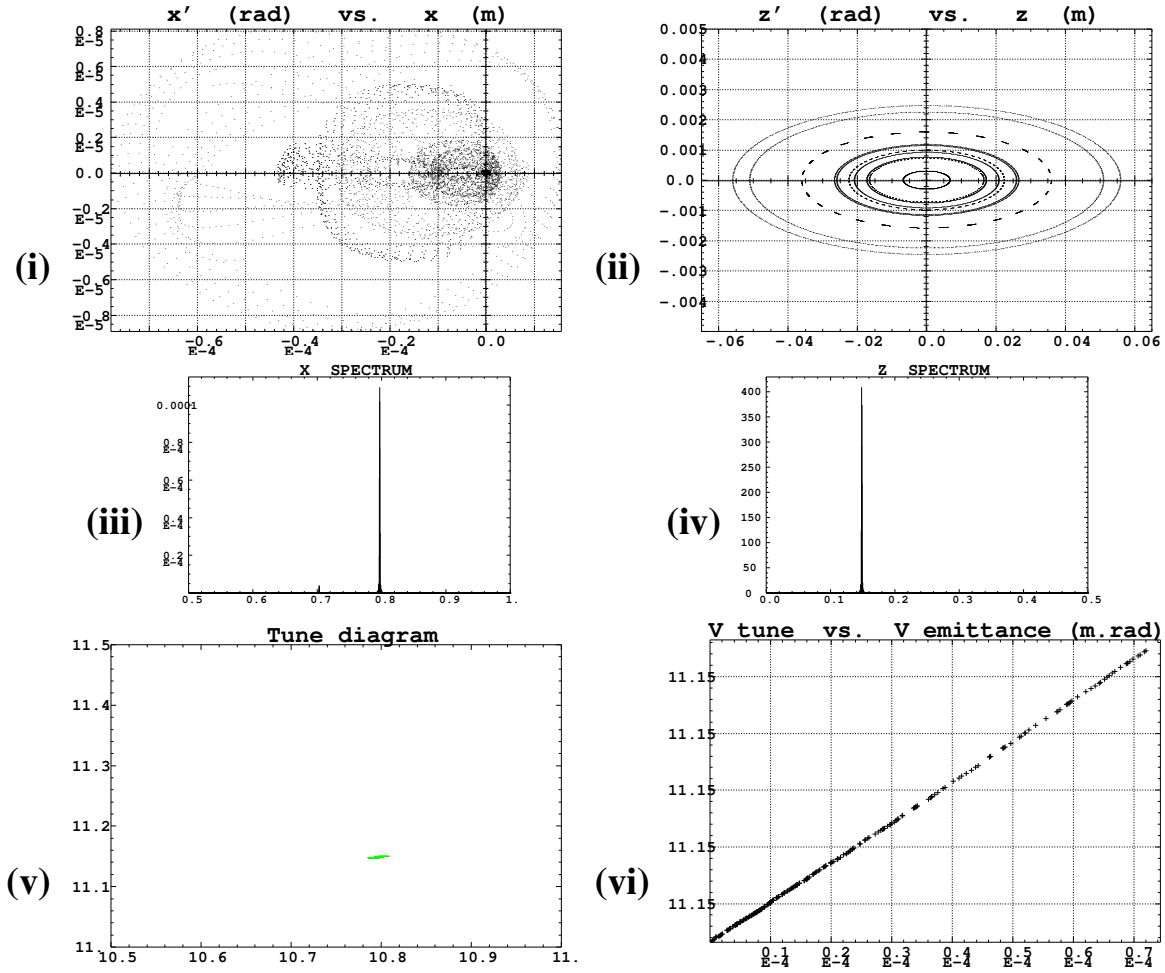

Figure 15: (i) Small induced horizontal motion of sample particles, due to the solenoids. (ii) Vertical motion, up to about $3\,\pi$ cm. (iii, iv) Specimen ν_x and ν_z spectra. (v) Tune diagram for the 200 particles, obtained by Fourier analysis. (vi) Amplitude detuning, ν_z as a function of ϵ_z/π.

4.1.3 4-D + $\delta p/p$ initial conditions

An 200-particle beam with initial $\epsilon_x = \epsilon_z = 3\,\pi$cm and $-1\% < \delta p/p < 1\%$, with distributions as shown in Fig. 13, is tracked for a few hundred turns. The transmission is close to 100%. Figs. 16-18 give the tracking results.

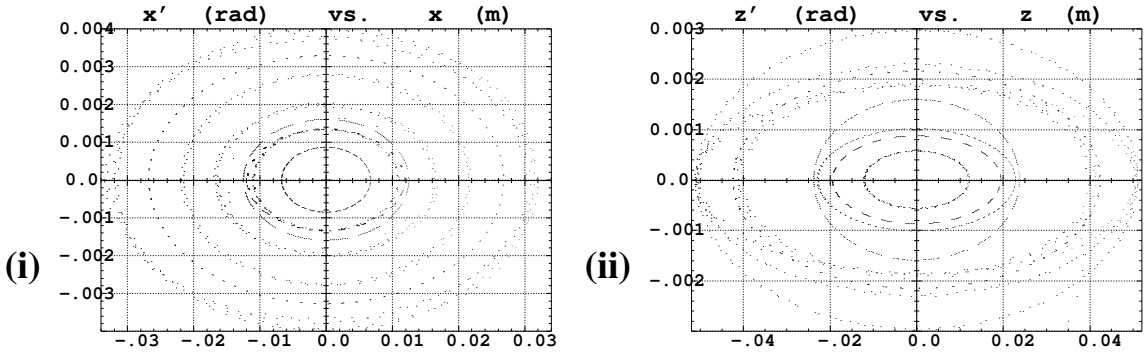

Figure 16: (i) Horizontal motion of sample particles. (ii) Vertical motion. The apparent mismatch of some ellipses stems from betatron mismatch of off-momentum particles.

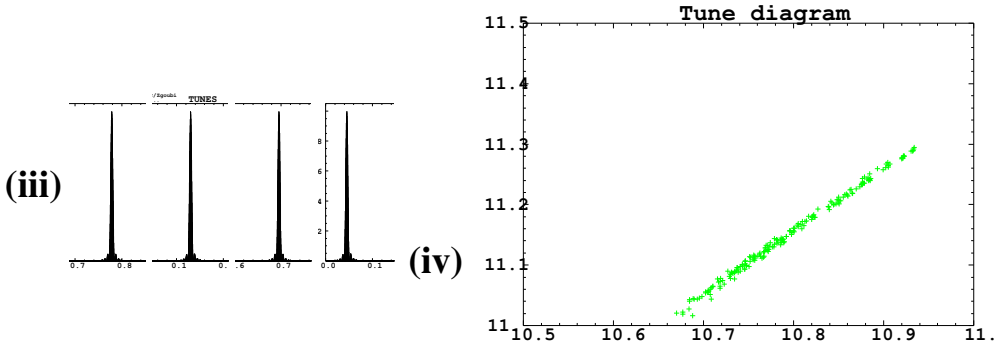

Figure 17: (iii) Sample spectra, respectively x/z/x/z from left to right, all showing a single peak, proof of negligible coupling. (iv) Tune diagram footprint, from Fourier analysis. The extent satisfies $\Delta\nu_{x,z} = \xi_{x,z}\delta p/p$ given $\xi_x \approx \xi_z \approx -15$.

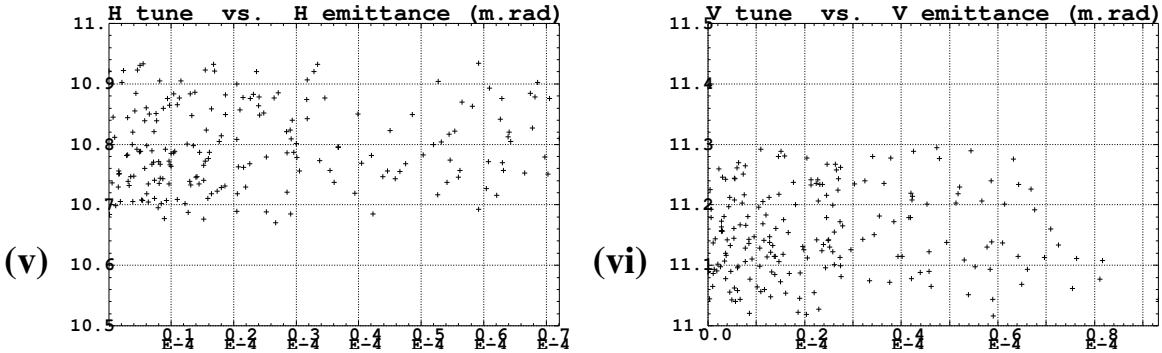

Figure 18: (v) Amplitude detuning, horizontal, ν_x as a function of ϵ_x/π (drawn from elliptical fit of each particle motion in phase-space) (vi) Amplitude detuning, vertical, ν_z as a function of ϵ_z/π.

4.2 Transmission, 4-D + $\delta p/p$, no sextupoles

4.2.1 $\epsilon_x = \epsilon_z = 3\,\pi$ cm (norm.), $\delta p/p = \pm 1\%$.

A 2000 particle beam is launched for 1000 turns around the ring. The initial conditions are those of Fig. 13, reproduced in of Fig. 19 for easier comparison with the tracking results. The transmission is 1942/2000 particles. In other words, the acceptance of the defect-free ring, chromaticity non corrected, is larger than $3\,\pi$ cm transverse, $\pm 1\%$ $\delta p/p$. The transmitted beam, after 1000 turns, is shown in Fig. 20, the momentum distribution remains that of Fig. 19, unchanged. Figs. 21, 22 show the satisfactory behavior of the horizontal and vertical phase-space motions and of the numerical tracking.

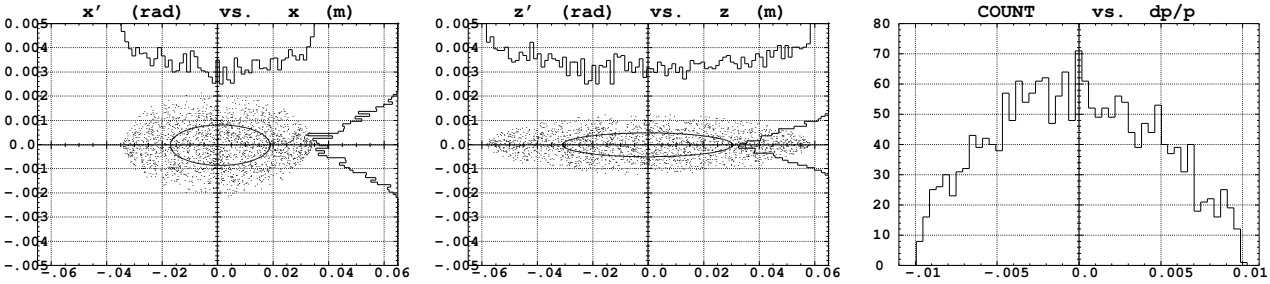

Figure 19: Initial conditions for transmission simulations. The local betatron functions are $\beta_x = 7.73$ m, $\beta_z = 22.7$ m, $\alpha_{x,z} = 0$, $D_{x,z} \approx 0$, $D'_{x,z} \approx 0$.

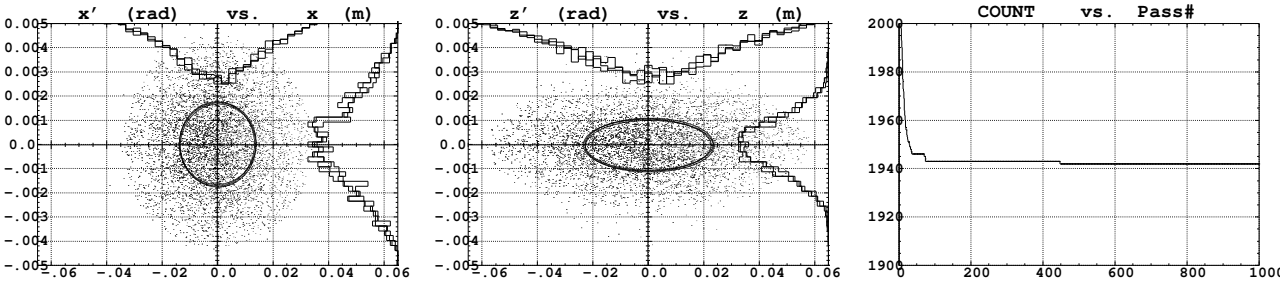

Figure 20: Left and middle : a superposition of (resp. H and V) phase spaces and projected densities at turns # 100, 500 and 1000 ; it can be observed that the emittance and densities practically do not change as turns proceed, meaning absence of sensible (numerical or real) diffusion effect. Right : number of particles transmitted vs turn number. Note : the apparent emittance increase, compared with Fig. 19, is the effect of momentum spread, in the absence of chromaticity corrections (adapted ellipse depends on $\delta p/p$).

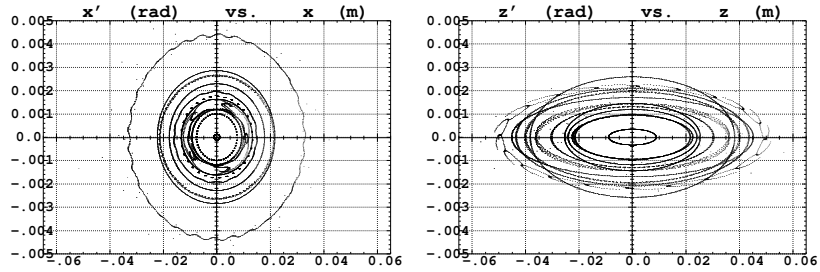

Figure 21: Sample multiturn tracking, some arbitrary particles with various H and V conditions. This shows the good behavior of the numerical integration (no evidence for non-symplectic behavior).

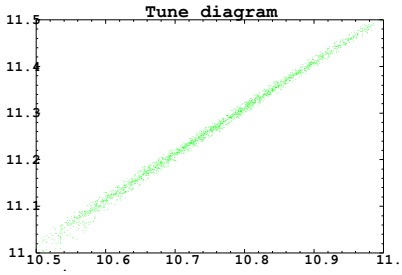

Figure 22: Beam footprint in the tune diagram, with extent due to the chromaticity, $\Delta\nu_{x,z} \approx -15\,\delta p/p$.

4.2.2 $\epsilon_x = \epsilon_z = 6\,\pi$ cm (norm.), $\delta p/p = \pm 4\%$.

A 10^4 particle beam is launched for 1000 turns around the ring, initial conditions schemed in Fig. 23. The transverse $6\,\pi$ cm (norm.) emittance value twice the requested one, the momentum bite is about four times larger than requested. The transmission is 5500/10000 particles, Fig. 24-left ; most of the losses occur during the first tens of turns, they are due to $\delta p/p$ induced resonant conditions (those parts of the beam that straddle harmful resonance lines). The transmitted beam, after 1000 turns, is shown in Fig. 24. It can be observed on Figs. 23 and Fig. 24, that the (x, x') and (z, z') transverse densities change their initial parabolic shape to an equilibrium bell shape, this is due to the $d\beta_{x,z}/dp/p$ in the absence of chromaticity correction, which also result in an apparent emittance increase. Figs. 25, 26 shows the satisfactory behavior of the horizontal and vertical phase-space motions and of the numerical tracking.

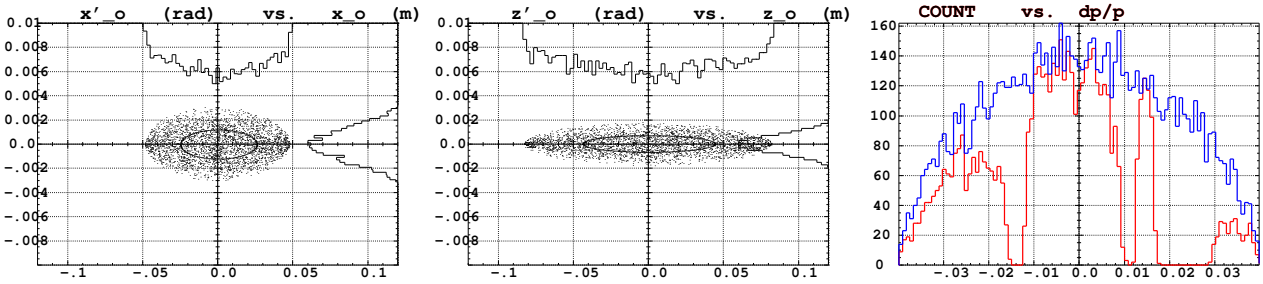

Figure 23: Initial conditions for transmission simulations, and transmitted momentum density (red histogram on the right). The local betatron functions are $\beta_x = 7.73$ m, $\beta_z = 22.7$ m, $\alpha_{x,z} = 0$, $D_{x,z} \approx 0$, $D'_{x,z} \approx 0$.

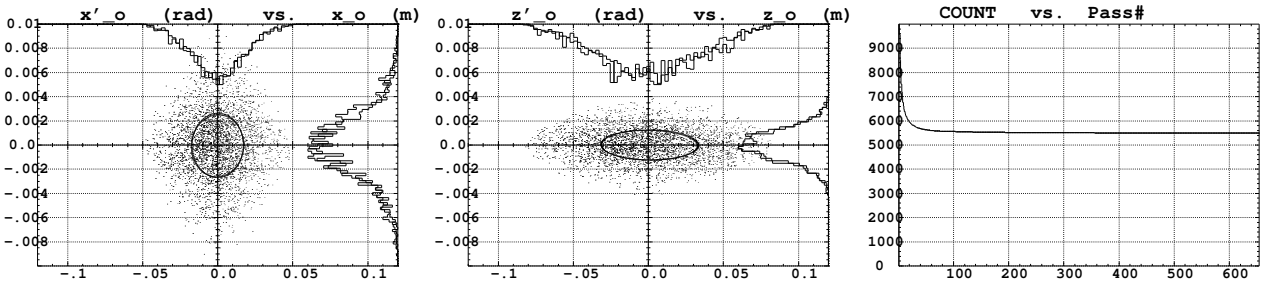

Figure 24: Left and middle : a superposition of (resp. H and V) phase spaces and projected densities at turns # 300 and 650 ; it can be observed that the emittance and densities practically do not change, meaning absence of sensible (numerical or real) diffusion effect. Right : number of particles transmitted vs turn number. Note : the apparent emittance increase, compared with Fig. 23, is the effect of momentum spread, in the absence of chromaticity corrections (adapted ellipse depends on $\delta p/p$).

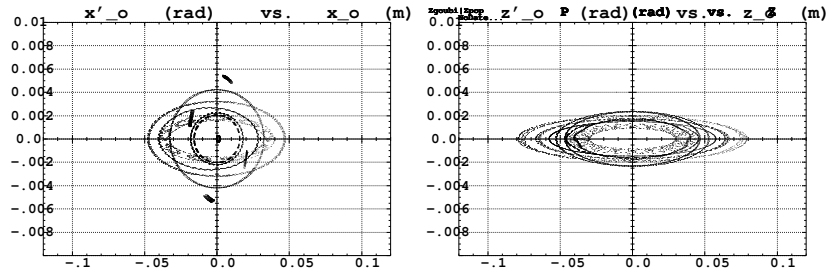

Figure 25: Sample multiturn tracking, height arbitrary particles with various H, V and $\delta p/p$ conditions, showing the good behavior of numerical integration (no evidence for prohibitive non-symplectic effects).

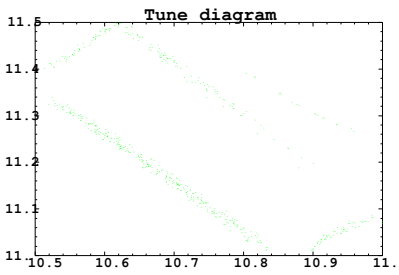

Figure 26: Beam footprint in the tune diagram, with extent due to chromaticity and coupling.

5 Transmission, 4-D + $\delta p/p$, chromaticity corrected

5.1 Chromaticity correction

Sextupole components are now introduced in the combined function dipoles of 10 arc cells in the 10 cell arcs, and in 15 cells in the 16 cell arc. This arrangement matches the $2\pi/5$ phase advance per cell, for cancellation of geometrical aberrations. They are tuned to reduce the *total* linear chromaticity in both planes (about twice the value stemming from the sole arcs) from -15 down to -1.
This correction scheme is simplistic, being comprised of only two families of sextupoles for compensation of ξ_x and ξ_z, regardless of possible improvements, by using a more sophisticated implementation. This is left to further more detailed investigations.
The effect of these sextupoles on closed orbit (up to $\pm 3\ mm$ in the horizontal plane, see App. 6) and its feed down on machine tunes are not corrected, they are left as they come.

5.2 Transmission

The initial conditions are, total emittances $\epsilon_x = \epsilon_z = 6\,\pi$ cm (norm.), $\delta p/p = \pm 4\%$ (Fig. 23). 630/1000 particles are transmitted, Fig. 28-right, most of the losses occur during the first tens of turns, rejection is both in $\delta p/p$ and emittance. The transmitted beam, after 1000 turns, is shown in Figs. 27 (momentum, red curve) and 28 (phase spaces). Comparison of Figs. 23-right and 27 shows the improvement in transmitted momentum bite resulting from the chromaticity correction. However the overall effect is limited, probably due to geometrical aberrations so introduced (reduction of DA).
Fig. 29 shows the satisfactory behavior of the horizontal and vertical phase-space motions and of the numerical tracking. Fig. 30 shows the beam footprint in the tune diagram, with extent due to chromaticity.

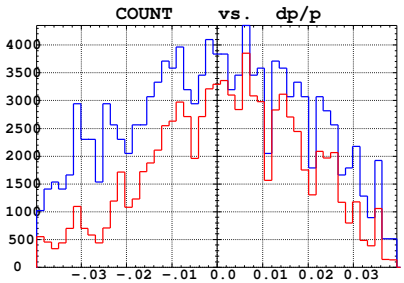

Figure 27: Momentum densities, initial (blue) and transmitted (red).

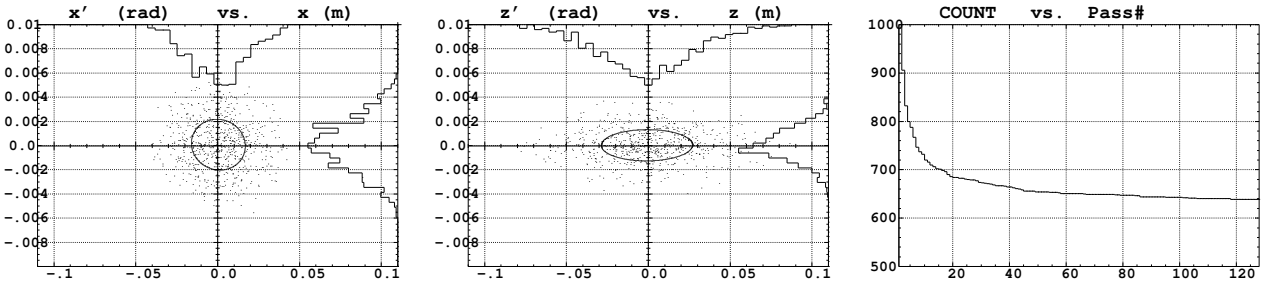

Figure 28: Left and middle : a superposition of (resp. H and V) phase spaces and projected densities at turns # 300 and 650 ; it can be observed that the emittance and densities practically do not change, meaning absence of sensible (numerical or real) diffusion effect. Right : number of particles transmitted vs turn number.

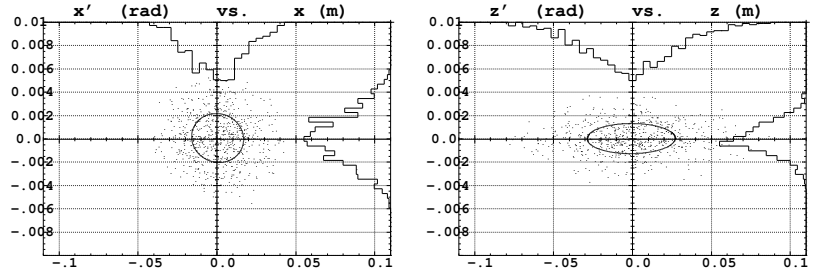

Figure 29: Sample multiturn tracking, arbitrary particles with various H, V and $\delta p/p$ conditions. It shows the good behavior of the numerical integration (no evidence for prohibitive non-symplectic behavior).

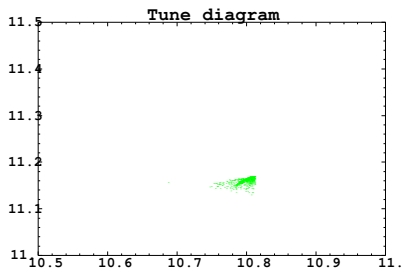

Figure 30: Beam footprint in the tune diagram, with extent due to chromaticity and coupling.

6 Conclusion

This tracking study shows that the principle of a triangle muon storage ring based on solenoidal focusing, and with apex angle consistent with two baselines, fulfills acceptance requirements.

Detailed investigations need be pursued, though, for instance on principle chromaticity corrections. This is left to further work and publications.

Appendix

Closed orbit induced by chromaticity sextupoles

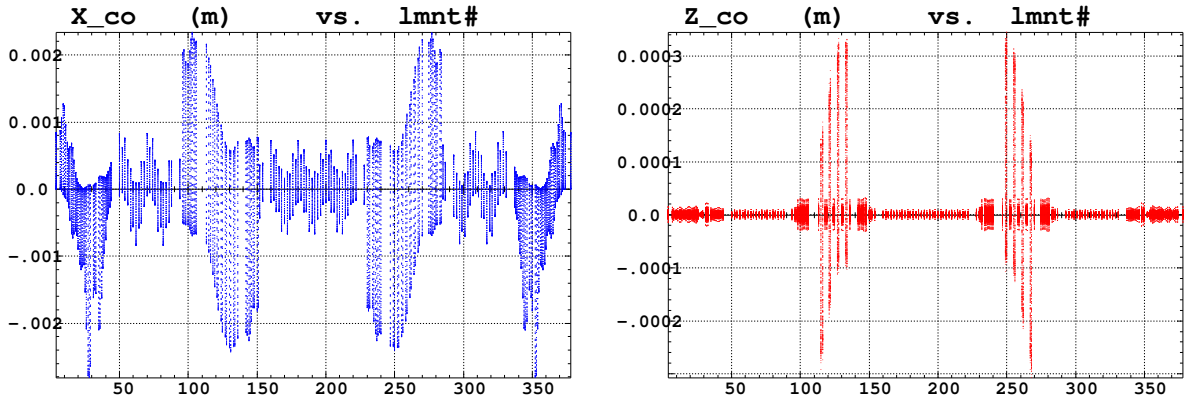

Extreme horizontal c.o. amplitudes of 2.4 mm and -2.8 mm are attained respectively in the decay straights and at ends of the collimation/tuning/RF straight (left Figure). In the absence of any correction.

The slight coupling introduced by the solenoids entails a c.o. excursion of ± 0.3 mm about, in the decay straights (right Figure).

References

[1] C. Johnstone et als., Muon storage rings for the neutrino factory, EPAC 2006.
[2] G. Rees, Stormu20 (20 GeV, μ+ and μ-, Isosceles Triangle, Storage Rings.), RAL, unpublished (2005).
[3] F. Méot, The ray-tracing code Zgoubi, NIM A 427 (1999) 353-356.
[4] The BETA code, J. Payet, F. Méot et *als.*, CEA/DAPNIA, Saclay.
[5] H. Grote, F. C. Iselin, The MAD Program, User's Reference Manual, CERN/SL/90-13 (AP) (Rev. 5), CERN, 29 April 1996.
[6] G. Leleux, Compléments sur la physique des accélérateurs, DEA de Physique et Technologie des Grands Instruments, rapport CEA/DSM/LNS/86-101, CEA, Saclay (1986).
[7] H.A. Enge, Deflecting magnets, in *Focusing of charged particles*, volume 2, A. Septier ed., Academic Press, New-York and London (1967).
[8] G. Leleux, Influence of quadrupole fringe fields on wave numbers, Tech. report 6-67/GL-FB, LAL, Orsay (2 Feb. 1967).